applied optics

Peering through the flames: imaging techniques for reacting aluminum powders

Ethan T. Zepper,[1] Michelle L. Pantoya,[1,*] Sukalyan Bhattacharya,[1] Jeremy O. Marston,[2] Andreas A. Neuber,[3] and Ronald J. Heaps[4]

[1]Mechanical Engineering Department, Texas Tech University, Lubbock, Texas 79409, USA
[2]Chemical Engineering Department, Texas Tech University, Lubbock, Texas 79409, USA
[3]Electrical Engineering Department, Texas Tech University, Lubbock, Texas 79409, USA
[4]Idaho National Laboratory, Idaho Falls, P.O. Box 1625, Boise, Idaho 83415, USA
*Corresponding author: michelle.pantoya@ttu.edu

Received 1 November 2016; revised 22 February 2017; accepted 23 February 2017; posted 23 February 2017 (Doc. ID 279601); published 17 March 2017

Combusting metals burn at high temperatures and emit high-intensity radiation in the visible spectrum, which can oversaturate regular imaging sensors and obscure the field of view. Filtering the luminescence can result in limited information and hinder thorough combustion characterization. A method for "seeing through the flames" of a highly luminescent aluminum powder reaction is presented using copper vapor laser (CVL) illumination, synchronized with a high-speed camera. A statistical comparison of combusting aluminum particle agglomerates imaged using various filtration techniques shows the effectiveness of the high-speed camera with a CVL diagnostic approach. When ignited by an electrically induced plasma, aluminum particles are entrained as solid agglomerates that rotate about their centers of mass and are surrounded by emitted, burning gases. The average agglomerate diameter appears to be 160 μm when viewed with standard illumination and a high-speed camera. However, a significantly reduced diameter of 50 μm is recorded when imaged with CVL illumination coupled with a high-speed camera and a 511 nm notch filter. These results indicate alternative imaging techniques are required to resolve the complexities of metal particle combustion.

OCIS codes: (140.3490) Lasers, distributed-feedback; (110.0110) Imaging systems; (160.0160) Materials; (240.0240) Optics at surfaces.

https://doi.org/10.1364/AO.56.002535

1. INTRODUCTION

Aluminum (Al) powder burns in ambient air at high temperatures, with an equilibrium adiabatic flame temperature thermodynamically calculated to be 3417 K [1] when reacting with pure oxygen (O_2). Aluminum powders can be mixed with solid oxidizers to form propellants, pyrotechnics, and thermites that have a variety of practical uses in industry [2,3]. High-speed imaging techniques are frequently used to observe combustion dynamics of aluminum-based energetic reactions. McNesby *et al.* [4] provide a thorough review of the evolution of imaging techniques for quantifying temperature, species, and visual combustion behaviors from explosive reactions. In fact, Densmore *et al.* [5] expands on the use of visual imaging techniques by employing color high-speed cameras to calculate temperatures of highly energetic reactions. However, combustion research typically uses monochromatic high-speed cameras to resolve reaction dynamics.

Figure 1 illustrates the intense brightness from an aluminum and copper oxide powder mixture reacting in a flame tube. The flame tube apparatus was introduced in [6] for quantifying flame speeds of thermite powder mixtures and consists of powder packed into a quartz tube. The tube shown in Fig. 1 has an inner diameter of 4 mm with 10 cm axial length and is loaded with 300 mg powder mixture uniformly distributed in the tube. Figure 1 includes an arrow indicating the direction of flame propagation, but little can be resolved about the powder combustion behavior that is masked by high luminescence. In fact, Sullivan *et al.* [7] consider alternative tube arrangements to refine flame speed measurements that may be affected by these highly luminescent powder reactions.

Aluminum powder also reacts in ambient air, and many have studied single particle burning behavior using imaging techniques [8,9]. Gill *et al.* quantified the size of burning metal particles using a single wavelength diode laser [10]. The authors showed that from the amplitude of the scattered light pulse when particles crossed the laser path, particle diameter can be measured *in situ* combustion [10]. This is an alternative approach to quantifying burning particle size without using

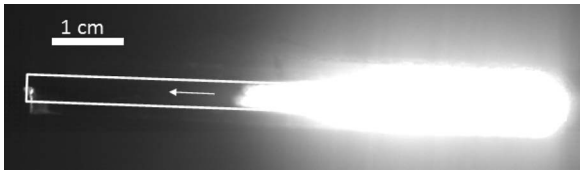

Fig. 1. Aluminum powder mixed with copper oxide powder burning in a flame tube and viewed through a 511 nm bandpass filter with a 1 nm FWHM. Note the white outline showing the tube location. The reaction was observed at 25,000 fps and 1280 × 720 pixels with an exposure time of 10 μs. Image shows oversaturation region as the reaction propagates from right to left in a quartz tube.

high-speed cameras. However, much research on Al particle combustion uses high-speed imaging systems and/or photodiodes to evaluate light emission [11,12].

Our preliminary observations of plasma-ignited Al powder combustion in air, using high-speed imaging up to 300,000 frames per second (fps), revealed peculiar particle dynamics (see Fig. 2). Particles were observed to ascend from the powder, oscillate, and subsequently burst or fragment violently, as seen in Fig. 2. The initial theory explaining these observations is based on a fluid-droplet model. This theory assumes that a droplet of molten aluminum lifts off the molten powder pool surface and proceeds to oscillate. The oscillations are a function of the interactions between the droplet surface tension, surrounding air, and the assumed trapped gases inside the droplet [13]. The subsequent "explosions" observed could be caused by trapped gases that ruptured the air-droplet interface, entraining particles into the surroundings. Particle size and pulsation frequency observations strongly support a molten droplet theory. However, due to the intensity of the visible radiation emitted from the combusting material, an accurate measurement of the particle agglomerate or droplet size could not be determined. These preliminary observations and assessments provide the motivation for developing improved visualization diagnostics.

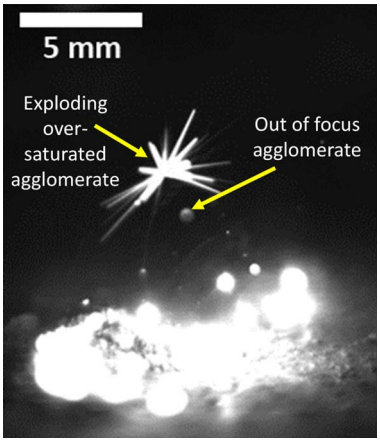

Fig. 2. Still frame image of plasma-ignited aluminum powder combustion in air recorded at 10,000 fps with an exposure time of 10 μs. Notice the bursting or explosion of a single agglomerate without external illumination or filtration, only the self-luminescence recorded. Other entrained particles are oversaturated.

It is interesting to note that others have observed a similar phenomenon as described above. For instance, Gottfried and Densmore examined close-up burning of a particle agglomerate ejected from an aluminum-based energetic composite [14]. They used a color Photron camera with a resolution of 512 × 512 pixels at a frame rate of 25,000 fps and observed a particle agglomerate (roughly the same size with scaling as above) burst apart several inches from the reactive material sample. Even with a different camera and operating conditions, the spatial resolution was not adequate to reproduce a full color image from the raw sensor data. However, time-resolved spectroscopy did reveal information about the composition of the burning particles. Also, the color sensor enabled thermal mapping of reactions, which is a useful additional component for energetic reactions [5,15].

Imaging diagnostics that employ narrowband laser radiation to distinguish against background radiation have demonstrated their usefulness many times over. In particular, lasers have been used previously to observe droplet combustion behavior because strong flame radiations mask the droplet surface [16,17]. Laser illumination also has been applied to solid combustion [4,18]. Methods including digital in-line holography (DIH) provide the ability to track particles in three dimensions while overcoming the visible light intensity of reacting aluminum particles emitted from a propellant strand [18]. The DIH technique uses laser illumination and a high-speed camera with a focal plane off-set from the objective focal distance. The recorded images are reconstructed numerically via computer program using the known focal off-set distance.

The objective of this work was to develop an imaging technique to overcome the visualization challenges of burning metallic powders by compensating for oversaturation while retaining image clarity of both the highly luminescent burning and dim, nonburning particle agglomerates. A copper vapor laser (CVL) was used to illuminate the field of view and overcome saturation from the particles. For comparison, identical tests were performed without the laser, using illumination from a halogen light. Five tests of each illumination technique were performed for statistical accuracy. The combination of highly luminescent burning particle agglomerates and nonburning agglomerates make external illumination necessary.

2. EXPERIMENTAL SETUP

A. Methods: an Overview

Experiments were designed to compare imaging of plasma-ignited Al powder using two imaging methods. The first uses a high-speed video (HSV) camera with standard halogen illumination and a neutral density (ND) filter on the camera lens (this method will be identified as HSV-ND for brevity). The second uses the same high-speed video camera and optics but is coupled with a copper vapor laser (CVL) and CVL notch filter (511 nm) on the camera lens (identified as HSV-CVL for brevity).

To analyze ignition, 25 mg of nano-scale Al particles were centered on an 8 × 8 cm blackened bulk aluminum target plate. The powder sample had an average diameter of 1 cm and uniform height. Ignition was achieved using an Electro-Technic Products BD-10AS high-frequency plasma generator to spark ignite the powder and was mounted 1 cm above the

powder sample. A Vision Research Phantom v2512 high-speed camera was fitted with an Infinity Photo-optical Company K2 Long Distance Microscope lens, with a focal depth of less than 1 mm and an effective pixel size of 16 × 16 μm. This coupled camera-and-lens system ensured that in-focus particles were within the plane and, therefore, their locations were known in space, as the plane depth was fixed. The camera was set to record at 15,000 fps, with the exposure time, t_{exp}, set to 20 μs. Note that the camera's enhanced dynamic range (EDR) was set to match t_{exp} for all experiments. A Hoya 4 × neutral density filter was attached to the camera lens to reduce the intensity of all wavelengths of light equally received by the camera sensor. This neutral density filter allows 25% of the original light to be transmitted to the camera sensor. The powder sample was placed consistently at 21.5 cm from the camera assembly. The HSV-ND illumination was provided by a QH-815 halogen light emitting 150 W.

For comparison, the tests performed with the CVL had a similar setup as above but with the addition of a 511 nm filter (∼1 nm FWHM, maximum of 70% transmission) in front of the neutral density filter. A signal with the same frequency as the capture rate is available through the "Burst" output on the camera. A BNC connector was attached to this output and linked to a Stanford Research Systems (SRS) Digital Delay/Pulse Generator. The signal was inverted and delayed by 60 μs before connecting to the "External Input" connection on an Oxford Lasers LS 20-50 CVL in order to synchronize the laser pulse rate and camera capture rate. The laser emits 0.9 mJ over a 30 ns pulse at a frequency of 15,000 Hz. The laser light was directed into a fiber optic cable and returned to its original 2.54 cm diameter through a collimator. The light was then focused onto the sample, as shown in Fig. 3. The recording speed remained at 15,000 fps; however, the exposure time, t_{exp}, was changed to 10 μs to time integrate less of the powder's self-luminosity. Note that the 15–20 ns CVL pulse duration becomes the effective exposure time for the laser pulse portion of the image. The laser timing switch was changed to sync with the camera, and the recording was repeated in the same manner as the HSV-ND tests.

B. Mechanism Justification

Figure 4 illustrates the spectral distribution of emissive power from the burning powder assuming a temperature of 3417 K and blackbody behavior. The curve in Fig. 4 was generated from Planck's Radiation Law [Eq. (1)], assuming an emissivity of one [19]:

$$I_\lambda(\lambda, T) = \frac{2hc^2}{\lambda^5}\frac{1}{\left(e^{\frac{hc}{\lambda k_B T}} - 1\right)}. \quad (1)$$

In Eq. (1), I_λ is intensity, h is Planck's constant, c is the speed of light, λ is wavelength, T is absolute temperature, and k_B is Boltzmann constant.

The validity of the HSV-CVL approach may be evaluated by comparing the intensity of the luminosity from the powder to the intensity of reflected laser radiation and the halogen light, respectively. The time-integrated intensity of the blackbody luminosity is show in Eqs. (2) and (3) as an energy per unit area, e:

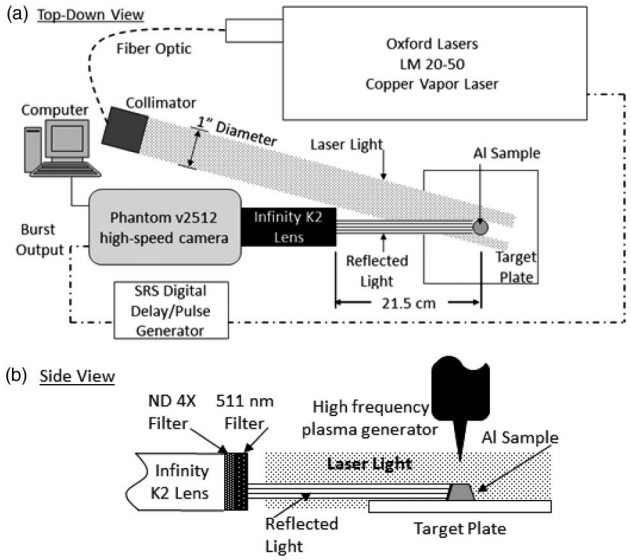

Fig. 3. (a) Top view of the CVL experimental setup. Phantom high-speed camera records event and provides signal of the recording speed, which is delayed and inverted through the SRS delay/pulse generator before driving the laser timing. The laser light is sent through a fiber optic cable and restored to the original 2.54 cm diameter beam through a collimator. The beam is focused on the aluminum powder sample observed through an Infinity K2 microscopic lens, and the event is recorded onto a computer. (b) Side view of CVL experimental setup. The aluminum powder sample is ignited by a high-frequency plasma generator. The CVL beam reflects from the sample surface and passes through a 511 nm filter as well as a ND filter attached to an Infinity K2 lens mounted on the high-speed camera.

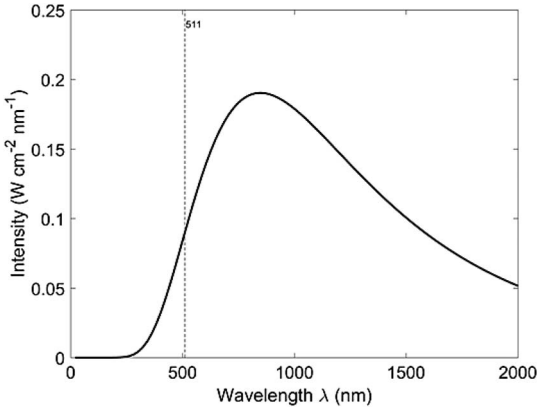

Fig. 4. Planck distribution for intensity from 3417 K reaction temperature, assuming a blackbody. The Hoya spectral filter position at 511 nm is indicated.

$$e_{powder} = P_{powder} t_{exp}, \quad (2)$$

where

$$P_{powder} = \tau \int_{\lambda_1}^{\lambda_2} I_\lambda(\lambda, T_{powder}) d\lambda. \quad (3)$$

The maximum spectral filter transmission is $\tau = 70\%$ (corresponding to the CVL 511 nm notch filter with maximum

70% transmission), λ_1 and λ_2 are 510.5 and 511.5 nm, respectively, covering the filter line width, and t_{exp} is 10 μs. Assuming the laser, as well as the halogen light, illuminate a $d =$ 25.4 mm diameter spot, their respective energy flux is calculated below in Eqs. (4) and (5). In both cases, a worst-case reflectivity $R = 5\%$ was assumed. Finally, the 150 W halogen output was matched to a filament temperature of 3200 K with a 0.8 cm^2 emission area, A:

$$e_{laser} = \tau \frac{RE_{pulse}}{\pi\left(\frac{d}{2}\right)^2}, \tag{4}$$

and

$$e_{halogen} = \tau \frac{R \cdot A}{\pi\left(\frac{d}{2}\right)^2} \int_{\lambda_1}^{\lambda_2} I_\lambda(\lambda, T_{halogen}) \mathrm{d} \cdot \lambda \frac{1}{\dot{F}}. \tag{5}$$

The laser pulse energy, E_{laser}, is 0.4 mJ, and $\dot{F}$ is the frame rate (15,000 fps). Note that the wavelength integration limits for the HSV-ND method (neutral intensity filters only) are set to 300 and 800 nm, respectively, in Eqs. (3) and (5). This wavelength range is considered typical for non-UV enhanced optical cameras/lenses.

The ratio of laser energy per unit area to energy per unit area radiated from the powder surface for the HSV-CVL setup results in Eq. (6):

$$\frac{e_{laser}}{e_{powder}} = 400. \tag{6}$$

The ratio of the halogen to powder energy per unit area for the HSV-ND setup is much lower, as shown in Eq. (7):

$$\frac{e_{halogen}}{e_{powder}} = 0.5. \tag{7}$$

Adding the spectral filter to the HSV-ND setup changes this ratio very little due to the closely matched temperatures of the halogen light filament and powder surface. The available intensity from the laser is about 400 times greater than the luminosity of the burning powder, compared with similar intensity levels of illumination and luminosity in the HSV-ND setup. Hence, a much finer definition of the power particle size may be obtained with the HSV-CVL setup.

C. Copper Vapor Laser

The Oxford Lasers LS 20–50 CVL is water-cooled, with an evacuated central tube, which is backfilled with a neon (98%) and hydrogen (2%) gas mixture. When started, the laser begins a heating cycle, which warms the thyratron (high voltage gas-phase switch) for the high-voltage electrical discharges that arc across the laser tube. Once warm, the electrical discharge begins heating the copper load on the bottom of the laser tube, melting it, and eventually filling the tube with copper gas. The light emitted from the laser is released in two wavelengths: 511 nm (green) and 578 nm (yellow), with a pulse duration of 15–30 ns. The short pulse duration acts as a strobe, freezing the motion, eliminating the streaks seen in Fig. 2. The column of light exits the laser through the optics mount, with a power measured at 19 W in the 2.54 cm diameter beam, and enters into a fiber optic cable. The fiber routes the light to the experiment on the laser table, where it is returned to its original diameter through a collimator. The output power from the collimator is measured at 13.6 W.

D. Materials

The Al powder is composed of spherical particles with a log-normal size distribution and average diameter of 80 nm. The particles were procured from NovaCentrix (Austin, TX) and were synthesized using an inert gas condensation technique [20]. The Al particles are surrounded by an alumina (Al_2O_3) passivation shell, formed at temperatures below 440 °C such that the shell is in an amorphous state with an average 4 nm thickness surrounding the aluminum core. All experiments were performed in an open ambient air environment (i.e., 23 °C, 1 atm, 20% relative humidity).

E. Plasma Ignition

The powder was ignited using a high-frequency plasma generator that provides 1–2 mJ of energy per pulse at a pulsation rate of 16 kHz. The power input to the powder was measured between 100 and 200 kW using fast voltage and current probes (for a single plasma discharge). The duration of an individual spark is approximately 30 ns, two orders of magnitude below that of the shortest capture rate used, such that plasma dynamics cannot be visualized.

F. Analysis

National instruments (NI) vision builder image processing software was used to locate and size the particles in the HSV-ND experiments due to the high contrast between the background and burning particles. However, in-focus particles cannot be distinguished in this method. For the HSV-CVL experiments, the contrast between the particles and the surrounding background was not high enough to use the software to measure particle size with accuracy, and the particle statistics for this case were calculated manually. In both methods, particle size was determined by locating two pixels along opposite edges with the steepest intensity gradient. It is also noted for the data reported on particle diameter measurements, uncertainty is estimated at 30 μm for both HSV-CVL and HSV-ND techniques.

3. RESULTS AND DISCUSSION

When viewing the recordings under self-illumination and halogen lighting (HSV-ND), the particles are observed to lift off of the powder surface. A portion of these "floating" particles begin to pulsate or oscillate, as seen in Fig. 5(a), and the majority of the particles eventually burst in an explosion-like separation as they undergo a violent atomization or fragmentation process. The HSV-CVL experiments show that the particles are, in fact, solid agglomerates, which may be held together by interparticle forces [Fig. 5(b)]. The agglomerates are nonspherical, and a "cloud" seen behind the agglomerate is proposed to be either a jet of alumina vapor rotating the agglomerate or the emitted burning vapor tracing the wake effect of the reacting agglomerate. In aluminum combustion models described by Washburn *et al.*, aluminum vapor released from within the shell of aluminum particles indicates the beginning stages of combustion [21]. The cloud observed in Fig. 5(b) also may be vapor phase reactants, intermediates, or product species. The agglomerates observed in the HSV-CVL experiments are more

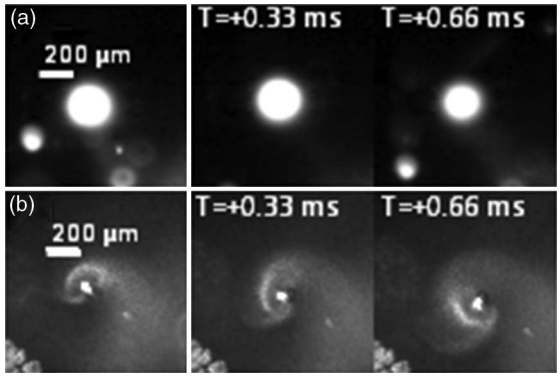

Fig. 5. Still frame images of aluminum particles using two experimental methods. Images (a) show HSV-ND: particle oscillations and a three-pixel difference in diameter. Images (b) show HSV-CVL illumination and a similar cluster of particles in rotation. Scaling and time stamps are shown.

easily resolved. While some of the centers of the agglomerates saturate, a distinct particle surface can be seen on the agglomerate edge in the HSV-CVL experiments.

One way to quantify the differences in visualization is by measuring particle size distributions using the two different imaging techniques. The oversaturation of the particles in the HSV-ND experiment is evidence that the measured particle diameter is a misrepresentation of the true diameter. Figure 6 shows the average particle size for both illumination methods. The HSV-ND experimental data have a higher percentage of large particle agglomerates, while the HSV-CVL experimental data appears to have two separate trend lines that meet close to 100 μm.

Another statistic is the quantity of particles emitted during the initial stages of ignition. Numerous particles and agglomerates ascend from the sample after the initial strike by the plasma; however, a distinct difference in size and focus can be seen between the HSV-ND and HSV-CVL experiments. Figure 7 shows the particle count statistics as a function of time. There are more particles tracked in the HSV-ND experiments

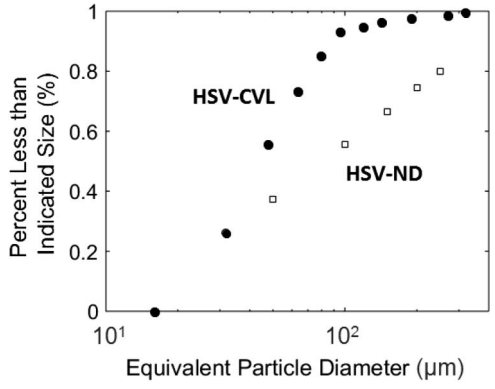

Fig. 6. Particle distribution for HSV-CVL (circle symbols) and HSV-ND (square symbols) experiments. The distribution shows agglomerate diameters (d_{agg}) between 10 and 300 μm for both HSV-CVL and HSV-ND indicating between 1.0×10^6 and 2.7×10^{10} individual particles with an average diameter of 100 nm (d_{Al}), respectively.

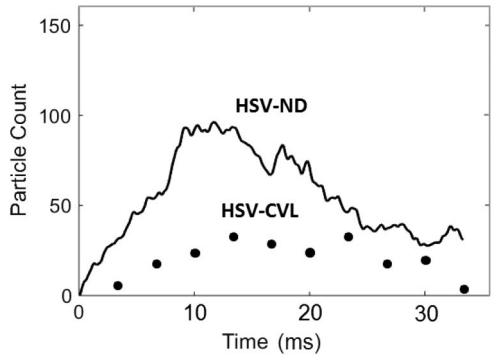

Fig. 7. Particle counts for HSV-CVL and HSV-ND illuminated experiments.

because the tracking software cannot delineate between in-focus and out-of-focus particles. Alternatively, only the in-focus particles were analyzed in the HSV-CVL experiments. In both experiments, the number of particles increased beginning with the first spark, and increased again, as some of the agglomerates burst into smaller particles. This can be seen between 9 and 20 ms for both illumination methods.

The average diameter of the burning Al particle agglomerates with respect to time is seen in Fig. 8. The general increase in the HSV-ND experiment can be attributed to an increase in out-of-focus burning particles as they exit the focal plane. For the HSV-ND experiments, the overall average corresponds to about 160 μm. The HSV-CVL agglomerate diameters were measured between two and six pixels on average, corresponding to 50 μm. The effective pixel size at this resolution was 16 μm. As a rule of thumb, the resolution is twice the effective pixel size, i.e., 32 μm.

When viewed without any filtration, measured diameters were far larger, averaging 0.9 mm. The large decrease in average diameter for the HSV-ND is a result of the addition of the 4× neutral density filter on the camera lens (e.g., allowing 25% light transmittance to the camera sensor). The residence times of the particles, defined as the duration the agglomerate is entrained prior to explosion, range from 10 to 40 ms.

The HSV-CVL illuminated agglomerates have a fairly consistent diameter of 50 μm, three orders of magnitude larger

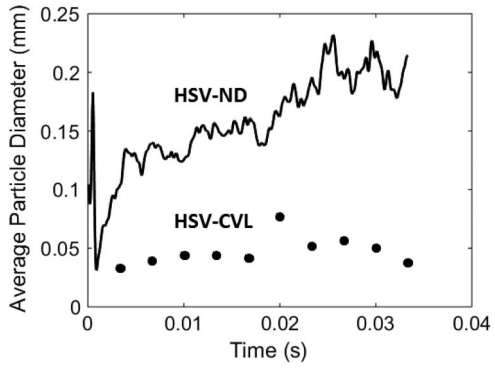

Fig. 8. Average particle diameter as a function of time for HSV-CVL and HSV-ND experiments. Without filtration on the camera lens, particle diameters measured on average 0.9 mm.

than the average measured particle diameter of 80 nm for the powder. Therefore, the observed particles are agglomerates entrained when the plasma superheated the air and ablated the powder, as seen in Fig. 9(a). In the HSV-CVL experiments, an opaque "cloud" is seen forming quickly after the initial plasma. This "cloud" is postulated to comprise entrained particles which begin burning, as shown by the increasing luminosity of the "cloud." In contrast, the "cloud" cannot be seen in the HSV-ND tests [Fig. 9(b)]; only the highly luminescent burning particles are visible.

The particles in the HSV-ND experiments display a peculiar phenomenon: agglomerates appear to pulsate. When the laser is employed in the HSV-CVL experiments, the pulsating spheres are revealed to be agglomerates of solid bodies, which rotate in a jet of burning vapor, as seen in Fig. 5(b). The pulsation/rotation frequencies are between 1000 and 4000 Hz, as shown in Fig. 10 as a function of agglomerate diameter. The cluster rotation accelerates with time to ensure conservation of angular momentum while it loses mass from combustion.

For the rigid body rotation, the corresponding frequency can be scaled as inversely proportional to the particle diameter:

$$f \propto \frac{v}{\pi d}. \tag{8}$$

In Eq. (8), v is the agglomerate velocity, d is the particle diameter, and f is the rotational speed in Hz. The particles observed in the HSV-CVL experiments have diameters of 50 μm and velocities of 0.5 m/s giving frequencies of approximately 1900 Hz in agreement with the observed frequencies in the range of 1000–4000 Hz.

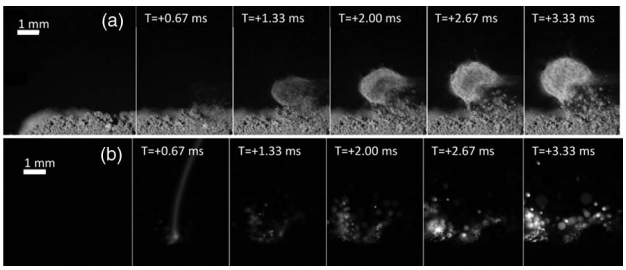

Fig. 9. (a) HSV-CVL illuminated particle dispersion and cloud growth, post spark. (b) HSV-ND illuminated particle dispersion, post spark.

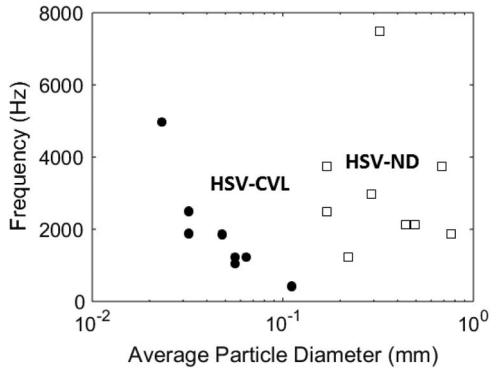

Fig. 10. Pulsation/rotation frequency for HSV-CVL and HSV-ND illuminated experiments.

The revelation of rotating solid clusters especially highlights the importance of CVL visualization. Oversaturation in regular imaging techniques causes combusting particles to appear oversized where details of the rigid body rotation are simply blurred. As a result, we see apparently spherical images undergoing ellipsoidal pulsation, which remains the only manifestation of the obscured rotating motion of asymmetric bodies. Such observation, however, can lead to drastically erroneous inference. It is natural to hypothesize an elliptically vibrating, suspended sphere to be a liquid droplet revealing its interfacial deformation waves [13,22]. Ironically, the wrong conjecture would even lead to the correct prediction of the frequency of oscillations, if one assumes entrapment of an air bubble inside the drop, created from the melting of inherently porous Al powder. The observed frequencies of the spherical images coincidentally match with the calculated values for the elliptical mode of oscillation in a multiphase domain of similar size. A recent theory [23] describing interfacial waves in bubble-laden drop yields 1800 Hz for the fluctuations in the perceived system with 35% void-fraction, which is a typical value for air residing in a loosely packed powder. Despite these promising agreements, granular details, provided by CVL imaging, force the abandonment of the liquid phase postulate in favor of a simpler and more accurate explanation. It should also be noted that brightness oscillations have been observed by others for aluminum particle combustion [24–26]. Most attribute brightness oscillations to intrinsic features of particle burning such as oscillations in burning rate or formation of oxide caps, rather than the result of forced or natural convective flows caused by gravity.

4. CONCLUSIONS

Aluminum particles burn with high light intensity in the visible spectrum. Copper vapor laser illumination has been coupled with high-speed video imaging (HSV-CVL) to shed new light on plasma-ignited aluminum powders burning with oxygen in the surrounding air. The same reactions were also visualized with neutral density filters (HSV-ND) for comparison. Reacting nano-aluminum powder entrains burning particle agglomerates, which rotate between 1000 and 4000 Hz, surrounded by the burning off-gases. A significant difference in particle diameter measurements was shown between the HSV-ND and HSV-CVL methods. The average size for the HSV-CVL experiments was 50 μm, as compared to the oversaturated particles in the HSV-ND experiments, measuring 160 μm. The particle residence times ranged from 10 to 40 ms. A luminescent cloud is made visible with HSV-CVL imaging and is suggested to comprise multiphase species.

Funding. Army Research Office (ARO) (W911NF-14-1-0250); Idaho National Laboratory (INL) (16-081).

Acknowledgment. The authors are thankful to the Army Research Office and grateful for the encouragement from our program manager, Dr. Ralph Anthenien. We thank Ryan Bratton and Kevin Hill for their assistance with the experiments.

REFERENCES

1. S. Goroshin, J. Mamen, A. Higgins, B. Tim, N. Glumac, and K. Herman, "Emission spectroscopy of flame fronts in aluminum suspensions," Proc. Combust. Inst. **31**, 2011–2019 (2007).
2. J. Giles, "Collateral damage," Nature **427**, 580–581 (2004).
3. L. L. Wang, Z. A. Munir, and Y. M. Maximov, "Thermite reactions: their utilization in synthesis and processing of materials," J. Mater. Sci. **28**, 3693–3708 (1993).
4. K. L. McNesby, B. E. Homan, R. A. Benjamin, V. M. Boyle, J. M. Densmore, and M. M. Biss, "Quantitative imaging of explosions with high speed cameras," Rev. Sci. Instrum. **87**, 051301 (2016).
5. J. M. Densmore, M. M. Biss, K. L. McNesby, and B. E. Homan, "High-speed digital color imaging pyrometry," Appl. Opt. **50**, 2659–2665 (2011).
6. B. S. Bockmon, M. L. Pantoya, S. F. Son, B. W. Asay, and J. T. Mang, "Combustion velocities and propagation mechanisms of metastable interstitial composites," J. Appl. Phys. **98**, 064903 (2005).
7. K. T. Sullivan, O. Cervantes, J. M. Densmore, J. D. Kuntz, A. E. Gash, and J. D. Molitoris, "Quantifying dynamic processes in reactive materials: an extended burn tube test," Propellants Explos. Pyrotech. **40**, 394–401 (2015).
8. R. Friedman and A. Macek, "Ignition and combustion of aluminum particles in hot ambient gases," Combust. Flame **6**, 9–19 (1962).
9. M. W. Beckstead, "Correlating aluminum burning times," Combust. Explos. Shock Waves **41**, 533–546 (2005).
10. R. J. Gill, S. Mohan, and E. L. Dreizin, "Sizing and burn time measurements of micron-sized metal powders," Rev. Sci. Instrum. **80**, 064101 (2009).
11. P. Lynch, H. Krier, and N. Glumac, "A correlation for burn time of aluminum particles in the transition regime," Proc. Combust. Inst. **32**, 1887–1893 (2009).
12. Y. Feng, Z. Zia, L. Huang, and X. Yan, "Experimental investigation on the combustion characteristics of aluminum in air," Acta Astronaut. **129**, 1–7 (2016).
13. J. C. Padrino, T. Funada, and D. D. Joseph, "Purely irrotational theories for the viscous effects on the oscillations of drops and bubbles," Int. J. Multiphase Flow **34**, 61–75 (2008).
14. J. L. Gottfried and J. M. Densmore, "Laser-induced breakdown spectroscopy of reactive materials doped with carbon nanoparticles," JANNAF J. Propul. Energy **6**, 23–35 (2013).
15. J. M. Densmore, B. E. Homan, M. M. Biss, and K. L. McNesby, "High-speed two-camera imaging pyrometer for mapping fireball temperatures," Appl. Opt. **50**, 6267–6271 (2011).
16. M. Huo, S. Lin, H. Liu, and C. F. Lee, "Study on the spray and combustion characteristics of water-emulsified diesel," Fuel **123**, 218–229 (2014).
17. H. Wu, K. Nithyanandan, T. H. Lee, C. F. Lee, and C. Zhang, "Spray and combustion characteristics of neat acetone-butanol-ethanol, *n*-butanol, and diesel in a constant volume chamber," Energy Fuels **28**, 6380–6391 (2014).
18. D. R. Guildenbecher, M. A. Cooper, W. Gill, H. L. Stauffacher, M. S. Oliver, and T. W. Grasser, "Quantitative, three-dimensional imaging of aluminum drop combustion in solid propellant plumes via digital in-line holography," Opt. Lett. **39**, 5126–5129 (2014).
19. F. P. Incropera, D. P. Dewitt, T. L. Bergman, and A. S. Lavine, *Fundamentals of Heat and Mass Transfer*, 6th ed. (Wiley, 2007), pp. 736–741.
20. D. Pesiri, C. E. Aumann, L. Bilger, D. Booth, R. D. Carpenter, R. Dye, E. O'Neill, D. Shelton, and K. C. Walther, "Industrial scale nano-aluminum powder manufacturing," J. Pyrotech. **19**, 19–31 (2004).
21. E. B. Washburn, J. A. Webb, and M. W. Beckstead, "The simulation of the combustion of micrometer-sized aluminum particles with oxygen and carbon dioxide," Combust. Flame **157**, 540–545 (2010).
22. W. H. Reid, "The oscillations of a viscous liquid drop," Quart. Appl. Math. **18**, 86–89 (1960).
23. S. Bhattacharya, "Interfacial wave dynamics of a drop with an embedded bubble," Phys. Rev. E **93**, 023119 (2016).
24. E. L. Dreizin, "Experimental study of aluminum particle flame evolution in normal and micro-gravity," Combust. Flame **116**, 323–333 (1999).
25. I. G. Assovskii, O. M. Zhigalina, N. A. Kiselev, G. P. Kuznetsov, and V. I. Kolesnikovsvinarev, "The effect of gravity on aluminum droplet combustion," Dokl. Phys. **44**, 409–412 (1999).
26. M. Marion, C. Chauveau, and I. GöKalp, "Studies on the ignition and burning of levitated aluminum particles," Combust. Sci. Technol. **115**, 369–390 (1996).